AL13 - Numerical Study and Industrial Testing on Optimizing New Anode Behavior by Changing Additional Voltage Strategies

Zhibin Zhao[1], Wei Liu[2] and Yafeng Liu[3]
1. Research Engineer of Science and Technology Management Department,
2. Director of Science and Technology Management Department,
3. Director of Aluminum Reduction Department,
Shenyang Aluminium& Magnesium Engineering & Research Institute Co., Ltd.,
Shenyang 110001, China
Corresponding author: sinzhao22@163.com

Abstract

Anode change is one of the necessary operations in modern aluminum electrolysis industry, which introduces huge impacts on thermal field, electric field, and cell stability. In this paper, a numerical model was developed to investigate the coupled thermo-electric-flow behavior after anode change in different locations (corner anodes or internal anodes). It was found that the effect of corner anode change on cell thermal balance is greater than that of internal anodes. It is possible to provide a larger additional voltage magnitude or a longer additional voltage time to increase the cell heat input and speed up the recovery rate of bath temperature. In this sense, two kinds additional voltage strategies were proposed and applied in corner anode change in an aluminum smelter. It was found that both strategies played a positive role in improving thermal and electrical behavior of new anodes without any thermal issues, especially for the one with longer additional voltage time.

Keywords: Aluminum reduction cell, anode change, thermo-electric-flow multi-field.

1. Introduction

The size and amperage of modern aluminum reduction cells have been continuously increasing during the past decades; now, there is even a clear evidence that some scholars have started discussing the possibility of 1000 kA cells [1]. As the heart of aluminum reduction cells, the size of anodes also shows an increasing trend. Because of anode consumption, the anodes need to be periodically replaced in 28 to 33 days. Therefore, anode change has become one of necessary operations in modern aluminum smelting industry.

The influence of new anodes (cold anodes) on aluminum reduction cells can be mainly concentrated in two aspects: a) The massive anodes with low temperature would introduce huge impact on the thermal balance of aluminum reduction pots, a new anode normally requires 16 to 28 hours of heating to gradually reach the electrolysis temperature [2]; b) The just settled new anodes would be covered by a layer of insulating solidified electrolyte, which generates notable horizontal current in the aluminum pad [3]. The magnetohydrodynamic (MHD) stability of the cell would be perturbed by this operation, and it also needs about 24 hours to pick up the full anode current. The adverse impact of anode change is embodied in the loss of current efficiency. In one such study, a current efficiency loss of 2.2 % was reported by one anode change [4].

In order to reduce the negative influence of anode change, EGA and Alcoa developed an anode preheating technology using external heating equipment [5-6]. However, there is no further public report on any industrial scale application. The extra investment of heating furnace may be a possible reason.

Actually, the picture of the behavior of new anodes is not very clear, which involves complex transient thermal and electric redistribution, bath flow, and its related solidification and melting phenomena. Most researches focused their attentions on thermal-electric coupling analysis [7] or just single flow field analysis [8]. Recently, a few scholars began to investigate the anode change process by coupling multi-field and bath solidification and melting together [2, 9]. How to improve the understanding of the anode changing process in view of multi-field and multi-level phenomena occurring, optimize the process, and reduce its impact on the steady-state operation is still one of the important emerging problems.

This paper describes a numerical model developed to investigate the coupled thermo-electric-flow behavior after an anode change at different locations (such as corner anodes or internal anodes). Then, two kinds of additional voltage strategies were proposed and applied in corner anode change to speed up its recovery rate. Both numerical analyses and industrial testing are presented in this paper.

2. Model Description and Case Setting

2.1 Model Description and Boundary Condition

A 500 kA cell containing 48 anodes was chosen as our physical geometry. In order to save computing time and resources, only the anodes and the bath layer were considered in this work. Figure 1 illustrates the simplified geometry and its boundary conditions.

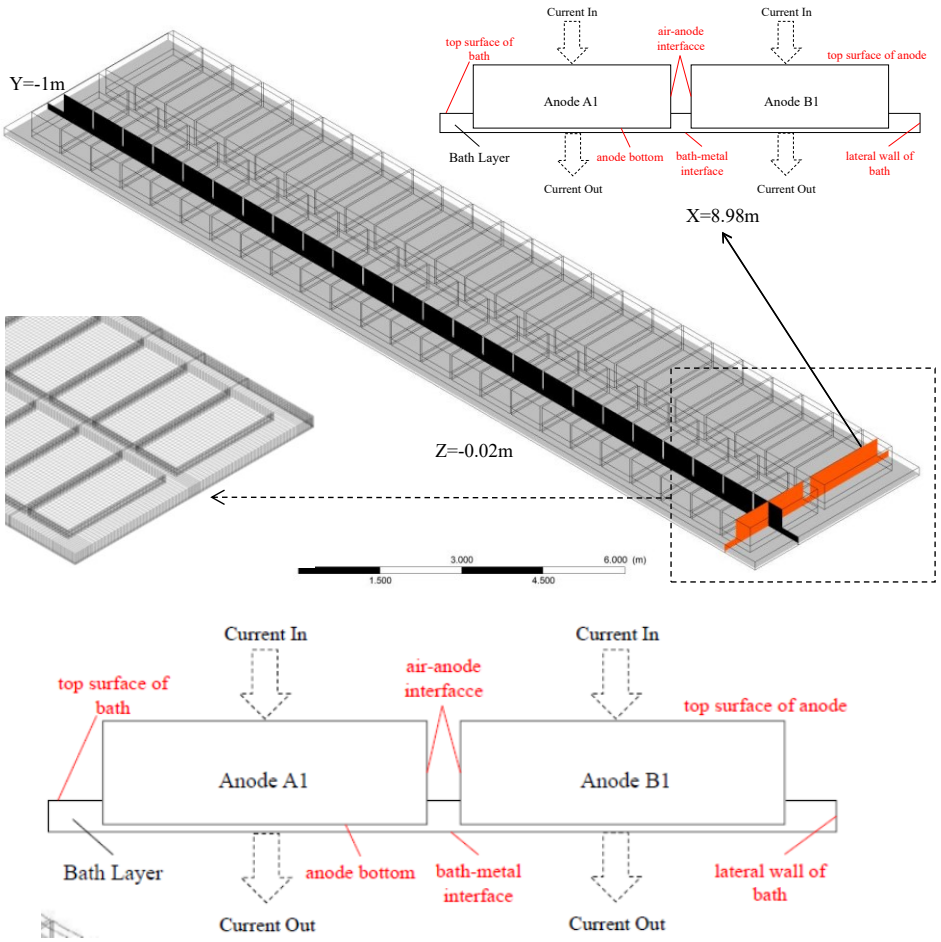

Figure 1. Geometry and boundary conditions. Bottom: upper right image magnified.

Electric boundary conditions: the current enters into the computing domain as current density vector from the top surface of the anodes and flows out of bath/metal interface where the potential was set to zero. The other boundaries were treated as insulated surfaces.

Thermal boundary conditions: A similar simplification as in a previous reference paper [2] was made for the anode covering material and the side materials. The heat transfer coefficients were set at the anode top and side surfaces, bath top and side surfaces, and bath/metal interface, respectively.

2.2 Governing Equations

2.2.1 Control Equations

The electro-magnetic coupling was determined from Equations (1) - (3); the electro-thermal coupling was analyzed with Equation (4); and the conservation of mass, momentum, and energy were solved using Equations (5) - (7).

$$\mathbf{E} = -\nabla\phi - \frac{\partial \mathbf{A}}{\partial t} \tag{1}$$

$$\mathbf{j} = \sigma\left(-\nabla\phi + \mathbf{u}\times\mathbf{B}\right) \tag{2}$$

$$\mathbf{F}_e = \mathbf{j}\times\mathbf{B} \tag{3}$$

$$Q = j^2/\sigma \tag{4}$$

$$\frac{\partial\rho}{\partial t} + \nabla\cdot\left(\rho\mathbf{u}\right) = 0 \tag{5}$$

$$\left(\frac{\partial\left(\rho\mathbf{u}\right)}{\partial t} + \nabla\cdot\left(\mathbf{u}\otimes\mathbf{u}\right)\right) + \nabla\cdot\left(\rho\mathbf{u}\right) = -\nabla P + \mu_{eff}\nabla^2\mathbf{u} + \mathbf{F}_e + \mathbf{F}_b + \mathbf{F}_p \tag{6}$$

$$\frac{\partial}{\partial t}\left(\rho H\right) + \nabla\cdot\left(\rho\mathbf{u}H\right) = \nabla\cdot\left(k_{eff}\nabla T\right) + Q \tag{7}$$

where variables in bold letters are vectors:

$\mathbf{E}$	Electric field
φ	Scalar potential
$\mathbf{A}$	Vector potential
t	Time
$\mathbf{j}$	Electric current density
σ	Electrical conductivity
$\mathbf{u}$	Fluid velocity
$\mathbf{B_0}$	Externally imposed magnetic field.
$\mathbf{F}$	Lorentz force
$\mathbf{B}$	Magnetic field
Q	Joule heating
ρ	bath density
$\mathbf{F_e}$	Lorentz force due to external magnetic field and internal electric field
$\mathbf{F_b}$	Buoyancy force
$\mathbf{F_p}$	Block effect in the mushy zone
k_{eff}	Effective thermal conductivity
H	Enthalpy
$\times$	Vector cross product
$\otimes$	Outer product.

2.2.2 Solidification and Melting

The bath solidification and melting process during anode changing was modeled by enthalpy-porosity method where the liquid fraction was calculated with Equation (8). If the bath temperature was lower than the solidification point of 1213 K (Ts), the liquid fraction (f1) was 0; if the bath temperature was higher than the liquidus point of 1221 K (Tl), the liquid fraction (f1) was 1.

$$f_l = \begin{cases} 0 & T < T_s \\ \dfrac{T - T_l}{T_l - T_s} & T_s < T < T_l \\ 1 & T > T_l \end{cases} \quad (8)$$

The block effect of solid electrolyte was considered in the defined mushy zone ($\overrightarrow{F_p}$). It was treated as a ‘‘pseudo’’ porous medium in which the porosity gradually decreased from 1 to 0 as the bath solidified, as shown in Equation (9).

$$\mathbf{F_p} = \frac{(1-f_l)^2}{f_l^3} A_{mush}\mathbf{u} \quad (9)$$

where A_{mush} is the mushy zone constant; a default value of 10000 was chosen here.

2.3 Case Setting

Four cases simulating anode changing were considered in this paper (listed in Table 1). A real additional voltage strategy (AVS) was chosen and applied in Case 1 and Case 2. The real additional voltage strategy was chosen from an operating smelter. Case 1 was to simulate the internal anode change of A1A2, and Case 2 was to represent a corner anode change of B15B16. The initial temperature of new anodes set was 50 ℃.

Two kinds of AVS were proposed in the optimization section. The first one was with larger additional voltage magnitude for Case 3, and the second one was with longer additional voltage time for Case 4.

Table 1. Cases studied in this paper.

Case	Additional voltage strategy	Changed anodes
1	+75mV_45min—+50mV_45min—+25mV_45min	A1A2
2	+75mV_45min—+50mV_45min—+25mV_45min	B15B16
3	+150mV_45min—+100mV_45min—+50mV_45min	A1A2
4	+75mV_45min—+50mV_90min—+25mV_135min	A1A2

3. Results and Discussion

3.1 . Thermal-Electric-Flow Behavior in Anode Changing

Magnetic data computed from Finite Element Analysis [10] were patched onto the bath domain as an externally imposed magnetic field. Before the anode change took place, adequate calculation was carried out until all parameters such as thermal and electrical distributions, flow characteristics, and ledge profiles reached a quasi-stable state. Figure 2 shows the velocity vector in the middle plane of ACD. It can be seen that the bath flow pattern and magnitude are similar to our previous simulation [11] without considering the solidification and melting process: there were two different size vortices, of which the vortex near the duct end ran counterclockwise, while the vortex near the tap end ran clockwise.

Figure 2 also shows the ledge profile on three planes (X = 8.98 m, Y=-1 m and Z=-0.02 m shown in Figure 1). A solid electrolyte layer of about 10-15 cm thickness was formed around the liquid phase, which can effectively protect side materials from the corrosive environment of liquid electrolyte. The solid ledge showed a reasonable profile, which agreed with industrial understanding.

The strategy of additional voltage for anode change is different for different aluminum smelters, but there exists a common purpose for improving energy input to heat new anodes and increasing ACD to maintain interface stable. This paper chose a real AVS that used in a smelter in this section: the first stage was to raise the cell voltage to +75 mV, lasting for 45 minutes, and in the second stage the cell voltage decreased to +50 mV, lasting for 45 minutes, and the final stage lasted for 45 minutes as well with the additional cell voltage of +25 mV.

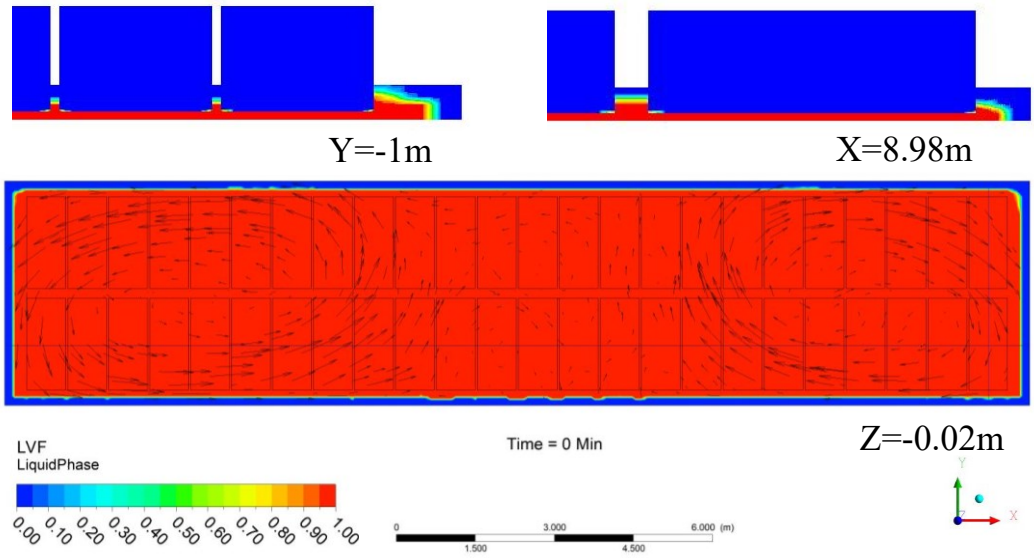

Figure 2. Bath flow on a horizontal plane in the middle of ACD and the ledge profiles around the liquid phase.

Figure 3 shows the distribution of joule heating Q in the middle plane of electrolyte at the first and third stages of additional voltage in Case 1 (A1A2). It can be seen that the joule heating Q of the first stage ranged from 0 to 3.37 x 10^5 W/m^3. The energy generation rate under new anodes was obviously smaller than that at other positions, which may be due to the low conductivity and low current density of the solidified electrolyte. The results showed that the heating rate of the half-cell within new anodes was slightly lower than that of the half-cell without changed anodes, which indicates the effect of cold anodes can be extended to the whole cell scale. The distribution of heating rate in the second and third stages was similar to that in the first stage, but the maximum heating rate reduced to 3.25 x 10^5 W/m^3 and 3.05 x 10^5 W/m^3, respectively. When the period with additional voltage was over, the heating rate returned to 0 to 2.83 x 10^5 W/m^3.

Figure 4 shows the recovery of temperature in the electrolyte region (cross section z = - 0.02 m) under new anodes. The bath temperature decreased to the lowest point of 1187 K (914 ℃) at 1.5 hours after the replacement of A1A2, then it began to slowly climb and finally reached the liquidus temperature in 12 hours. The calculation for this case was highly intensive and lasted for several days, so 5 hours of data were used in the following work for comparison.

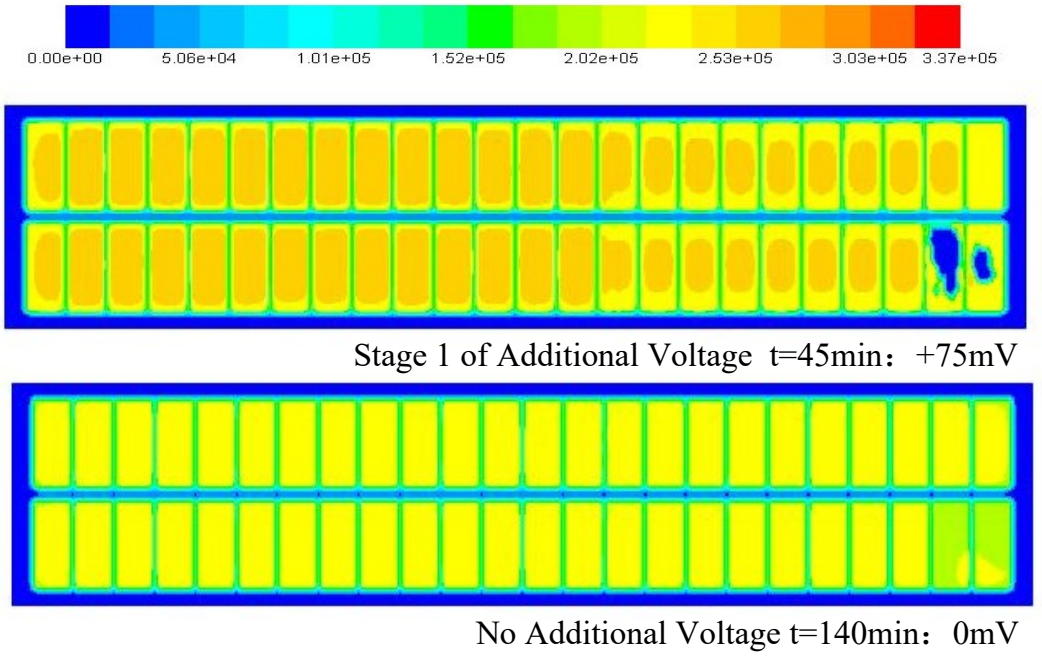

Figure 3. Joule heating Q at the first and third stages of additional voltage in Case 1.

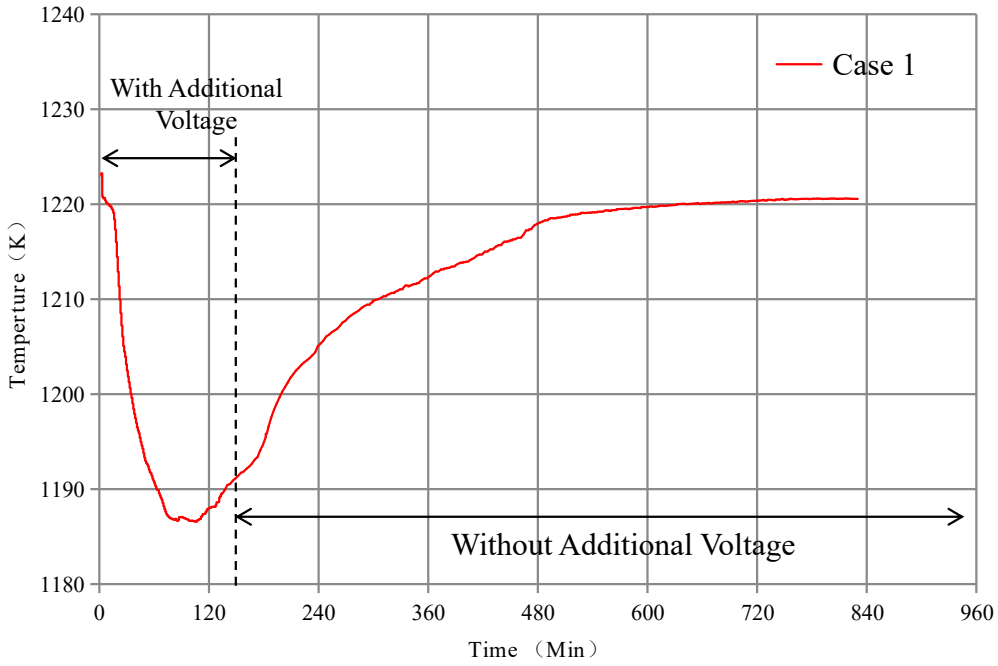

Figure 4. Temperature recovery of electrolyte under new anodes in Case 1.

3.2 Comparison of Anode Change in Different Locations

In industrial pots, the anodes A1A2, B1B2, A23A24, and B23B24 are located in pot corners, and their current pick-up rate is often slower than that of anodes at internal positions. Figure 5 shows a typical anode current distribution, and the current of corner anode was still less than 50 % after 48 hours following B23B24 change. In order to further confirm that this is a regular phenomenon, Figure 6 is given and shows the current pick-up rate of corner anodes and internal anodes after

change in an aluminum smelter. From the slopes of linear fitting, it can be seen that the current pick-up rate of corner anode change was about 5 % lower than that of internal anode change.

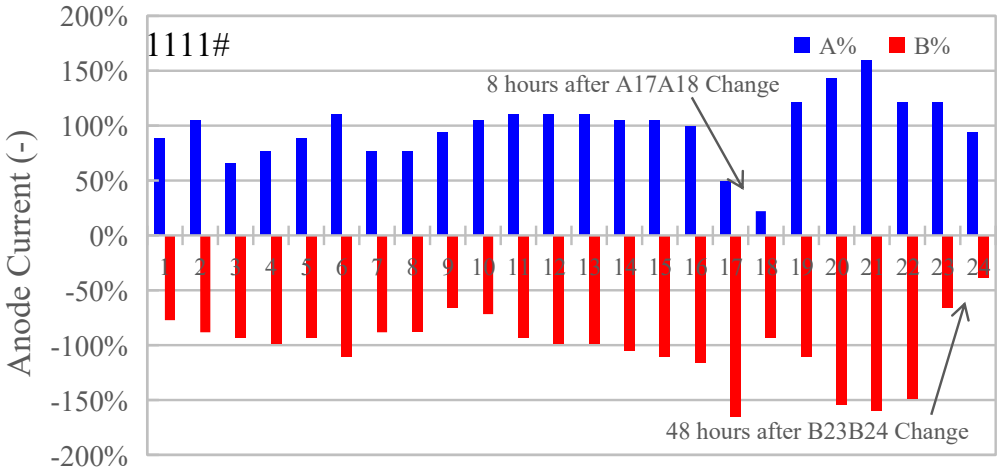

Figure 5. Typical anode current distribution after 48 hours following corner anode change.

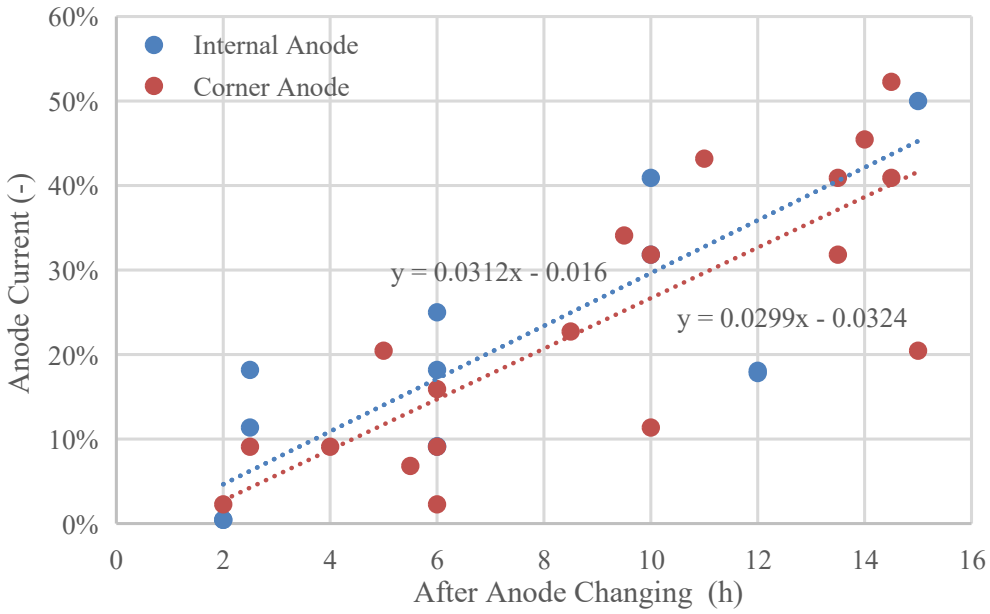

Figure 6. Comparison of current pick-up rate of corner anodes and internal anodes after change (data from an aluminum smelter).

Figure 7 illustrates the curves of temperature recovery under traditional AVS by changing corner anodes A1A2 and internal anodes B15B16 predicted by the numerical model presented above. The bath temperature in the corner anode case dropped to 1187 K (914 ℃) in about 1.5 hours, while the temperature of internal anode case decreased to a minimum temperature of 1201K (928 ℃) after 2.2 hours. The lowest temperature was 14 ℃ higher than that of corner anodes. This phenomenon can be attributed to two possible reasons: one is the heat dissipation from internal anodes is obviously smaller than that from corner anodes due to their locations; the other reason is the bath flow which would bring lots of energy and heat the new anodes for a better recovery of temperature and current.

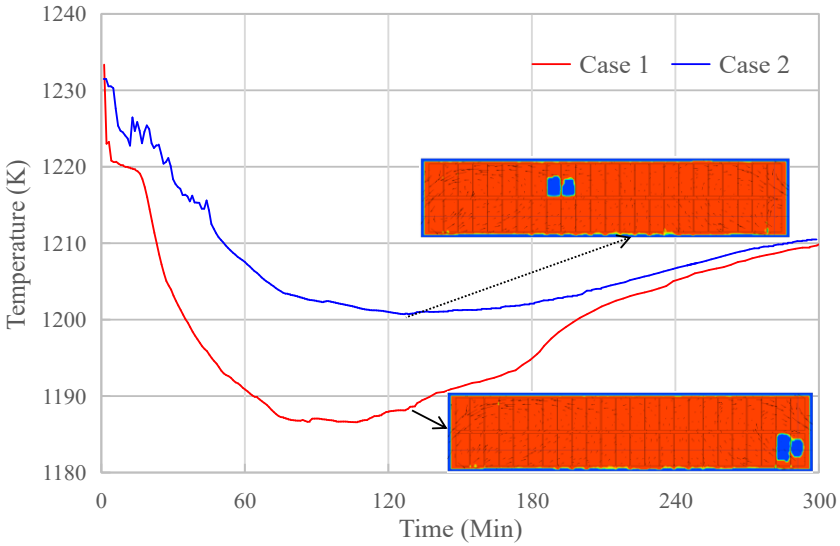

Figure 7. Temperature recovery in the electrolyte under new anodes in Case1 and Case 2.

3.3 Optimization Work on Anode Change

3.3.1 Numerical Analysis

To remedy the problem mentioned in section 3.2, some optimization work was tried on additional voltage to improve the behavior of new anodes. Figure 8 shows two curves of temperature recovery for corner anodes A1A2 with different kinds of AVS. Case 3 was the case with a larger additional voltage magnitude (Additional Voltage Strategy A - AVS_A), and Case 4 was the case with a longer additional voltage time (Additional Voltage Strategy B - AVS_B).

The numerical simulation showed that both additional voltage strategies played a positive role on the recovery of liquid temperature. The effect of AVS_A was seen in a short time in Case 3. The minimum temperature reduced to 1200 K (927 ℃), which was clearly higher than 1195 K (922 ℃) of Case 4 and 1187 K (914 ℃) of the base Case 1. At longer times, the effect of AVS_B in Case 4 became clear, and the electrolyte below new anodes recovered to a higher temperature than that in Case 3 after 4 hours.

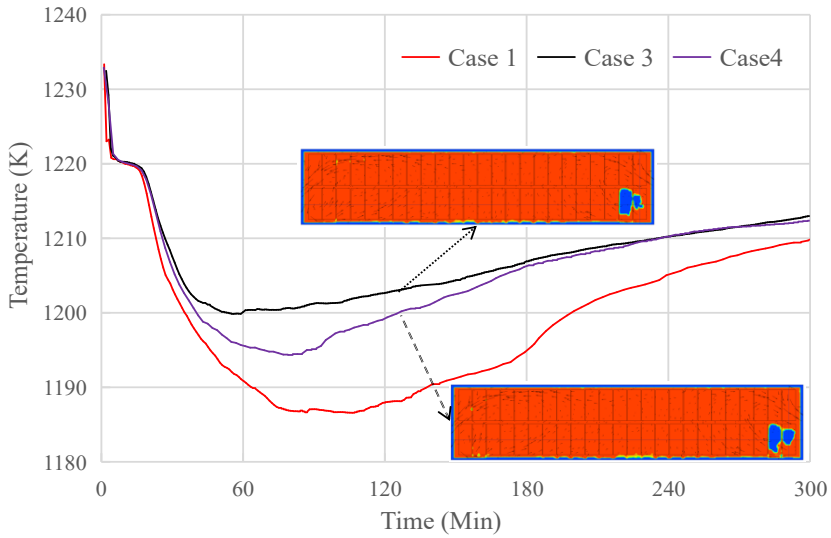

Figure 8. Temperature recovery curves for corner anodes A1A2 with two kinds of AVS.

3.3.2 Industrial Testing

The industrial trials were carried out after the numerical work of the last section. Figure 9 and Figure 10 show the current pick-up for corner anodes under AVS_A and AVS_B. In the test for AVS_A, Pots 1237# and 1238# were test cells and Pots 1239#, 1240#, and 1241# were reference cells. In the test for AVS_B, Pots 1235# and 1236# were test cells and Pots 1232#, 1233#, and 1234# were reference cells.

The smelter usually makes some adjustments for the anodes with an abnormal pick-up current after 16-20 hours of anode change, thus the data at 16 hours after anode change were chosen in this section.

It can be seen that the current pick-up rates of test cells with two AVSs were higher than that of reference cells. According to the fitted-lines, the pick-up rate of anode current in test cell A was 8 % higher than that in reference cells, and the current pick-up rate in test cell B was 11 % higher than that in reference cells. The effect of AVS_B was more effective than that of AVS_A.

Since the additional voltage was applied to the pot at the whole cell level in a short period, it was necessary to track the temperature change because a sudden increase in heat input would destroy the thermal balance of test pots. Figure 11 and Figure 12 show the trends of electrolyte temperature at the tap-end hole within 24 hours after anode change. There was no clear difference between the test cells and reference cells. The bath temperature varied in reasonable values and returned to the level before anode change after 24 hours. There was no issue the thermal balance of the test cells.

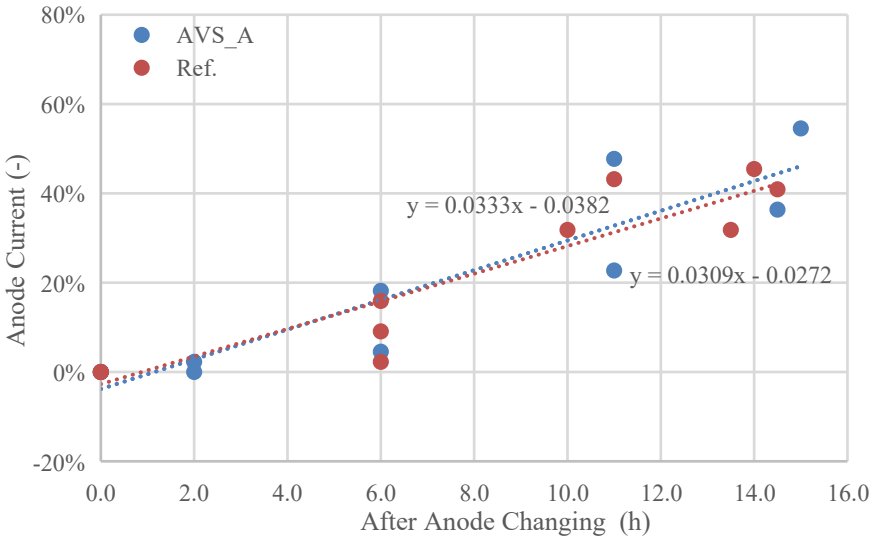

Figure 9. Current pick-up lines for corner anodes under the AVS_A (measured data).

Considering the aluminum reduction cell is sensitive to instantaneous heat input, the optimization trial of AVS_B may be a better choice. To all pots in this smelter, the second additional voltage strategy was applied for their corner anode change.

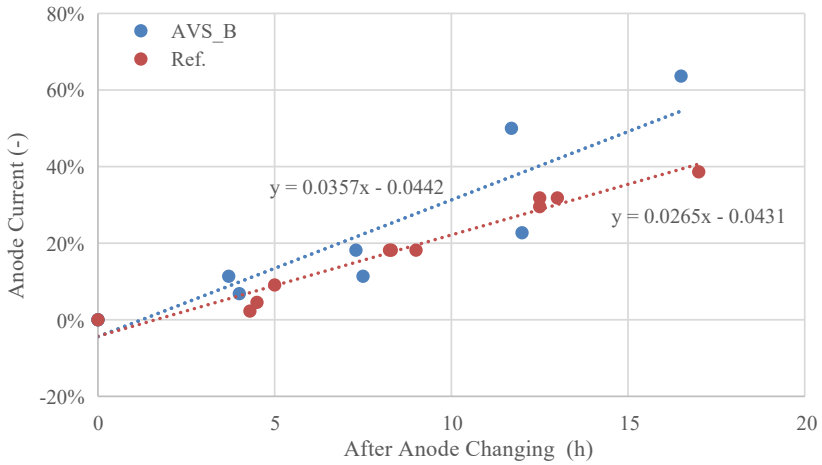

Figure 10. Current pick-up lines for corner anodes under the AVS_B (measured data).

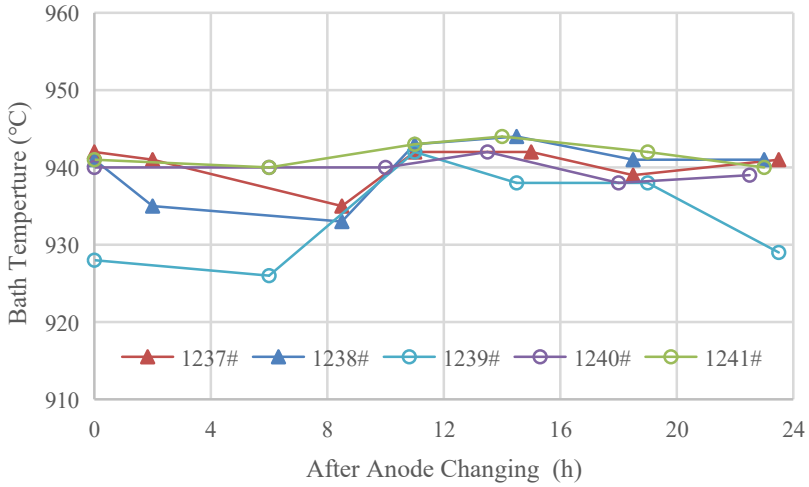

Figure 11. Bath temperature after corner anode change under the AVS_A (measured data).

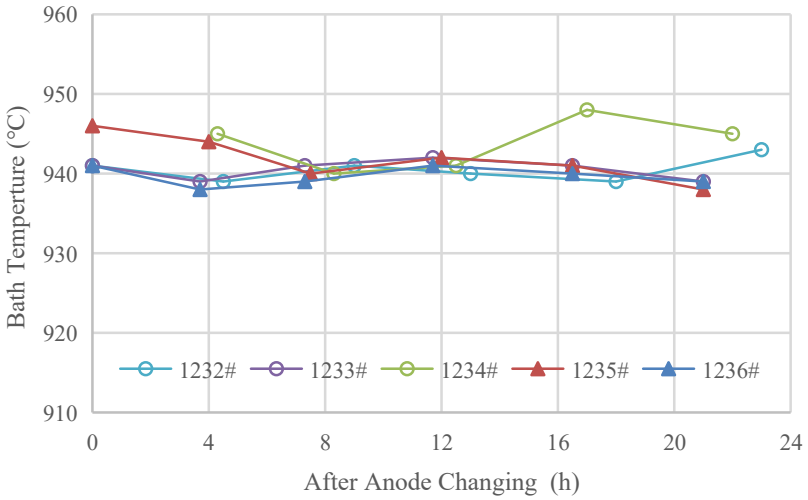

Figure 12. Bath temperature after corner anode change under the AVS_B (measured data).

4. Conclusions

A numerical model for anode change was developed by considering the solidification and melting process of electrolyte. The model can simulate and analyze the heat balance, electric field redistribution and bath flow after anode change. The following main conclusions can be drawn from this work:

(1) Both industrial measurement and numerical analysis showed that the impact of corner anode change was greater than that of internal anode change. The temperature recovery and current pick-up rate could be improved by increasing the magnitude or time of additional voltage.
(2) The two additional voltage strategies had no obvious negative effect on the thermal balance of the aluminum reduction cell, but the one with longer time gave better results. Based on the industrial test, the aluminum plant extended this additional voltage strategy with longer time for corner anode changing to the whole potline.
(3) The method of applied different additional voltage for different locations can be extended to other kinds of aluminum reduction cells, which may play positive role in the design and optimization of industrial anode change strategy.

5. References

1. Marc Dupuis and Barry Welch, Designing cells for the future–Wider and/or even higher amperage, *Aluminium* 2017(1-2), 45-49.
2. Q. Wang, B. Li, M. Fafard. Effect of anode change on heat transfer and magneto-hydrodynamic flow in aluminum reduction cell. *JOM* 2016(68): 610-622.
3. Valdis Bojarevics and Sharnjit Sira. MHD stability for irregular and disturbed aluminium reduction cells, *Light Metals* 2014, 685-690.
4. R.T. Poole, C. Etheridge, Aluminum reduction cell variables and operations in relation to current efficiency, *Light Metals* 1977, 163-182.
5. Otavio Fortini et al., Experimental studies of the impact of anode pre-heating, *Light Metals* 2012, 595-600.
6. Ali Jassim, Sergey Akhmetov and Barry Welch, Studies on anode pre-heating using individual anode signals in Hall-Héroult reduction cells, *Light Metals* 2016, 623-628.
7. F. Wang, Q. Zhang, W. Liu, X. Yang, D. Zhou, Application of numerical simulation technology to heat balance diagnosis in aluminum reduction pot, *Light Metals* 2019(1), 25-28 (In Chinese).
8. X. Qi, N. Feng, J. Cui, Effect of anode change and metal height on flow field of metal pad in aluminum reduction cells, *Chinese Journal of Nonferrous Metals* 2005(15), 485-489.
9. Hongliang Zhang et al., Study on 3D full cell ledge shape calculation and optimal design criteria by coupled thermo-flow model, *Light Metals* 2018, 587-596.
10. A. Zhou, H. Hu, X. Wwang, D. Chen. Magnetic field numerical simulation and testing research of SY500 kA aluminum reduction pots, *Light Metals* 2019(3): 25-28 (In Chinese).
11. Z. Zhao, S. Tao, W. Liu, X. Yang, Analysis on numerical simulation and industrial measurement of alumina concentration distribution in large-amperage prebaked aluminum reduction cell, *Light Metals* 2019(07): 20-24 (In Chinese).